Transient Weighted Moving-Average Model of Photovoltaic Module Back-Surface Temperature

Matthew Prilliman, Joshua S. Stein [2], Daniel Riley, and Govindasamy Tamizhmani

***Abstract*—Accurate modeling of photovoltaic (PV) performance requires the precise calculation of module temperature. Currently, most temperature models rely on steady-state assumptions that do not account for the transient climatic conditions and thermal mass of the module. On the other hand, complex physics-based transient models are computationally expensive and difficult to parameterize. In order to address this, a new approach to transient thermal modeling was developed, in which the steady-state predictions from previous timesteps are weighted and averaged to accurately predict the module temperature at finer time scales. This model is informed by 3-D finite-element analyses, which are used to calculate the effect of wind speed and module unit mass on module temperature. The model, in application, serves as an added filter over existing steady-state models that smooths out erroneous values that are a result of intermittency in solar resource. Validation of this moving-average model has shown that it can improve the overall PV energy performance model accuracy by as much as 0.58% over steady-state models based on mean absolute error improvements and can significantly reduce the variability between the model predictions and measured temperature times series data.**

***Index Terms*—Performance analysis, photovoltaics (PV), renewable Energy, thermal modeling.**

I. Introduction

THE continued growth of the photovoltaic (PV) contribution to the overall global energy profile has led to growing interest among researchers and system developers in improved PV performance models. PV performance is primarily driven by changes in irradiance, but operating temperature also has a significant effect on the power output, with a typical drop of approximately 0.3–0.5%/°C, depending on the PV cell technology [1]. The current state of PV module thermal modeling is dominated by steady-state models that assume that the module is in equilibrium with the surrounding environment, which is characterized by the plane-of-array irradiance, ambient air temperature, wind speed, and wind direction [2]–[7]. Previous works have shown that these models are sufficiently accurate for longer timesteps (i.e., > hourly) that consider averages over the interval [8]. However, reducing the time interval to account for irradiance and wind vector fluctuations at the PV array site reveals large modeling errors. This phenomenon is particularly evident during periods of large high-frequency changes in the plane-of-array irradiance of a PV system because of partly cloudy conditions. Since steady-state models vary directly with irradiance, large irradiance changes at data intervals such as 1-min result in corresponding predictions of step changes in the module temperature. Model predictions at this frequency may be indicative of no actual thermal behavior of fielded modules, which have inherent thermal mass that reduces the rate of change of module temperature. Overestimation of low irradiance performance and insufficient modeling of inverter clipping have been shown to be common in hourly performance models [9], [10]. In addition, modeling PV performance for energy storage system control and short-term forecasts of PV production require short timestep simulations and a transient model of module temperature [11].

Resistance–capacitance (*RC*) circuit analysis has been used for transient temperature modeling of PV modules [12], [13]. *RC* models treat the module as a network of circuits operating in parallel and in series, with thermal resistances operating in series and thermal capacitances operating in parallel. Such models require precise measurement or definition of the thermal and physical properties (e.g., conductivity, heat capacity, dimensions) of each material within the PV module, and these properties are rarely available (i.e., spec sheet). This difficulty in obtaining in-depth thermal properties of each layer hinders adoption of such a model by PV system modelers.

Previous work to develop transient thermal models has also been based on solving a physical heat transfer model with equations designed to balance energy by representing convection, radiation, and electricity production from a PV module at a given instant. Jones and Underwood [14] developed a transient thermal model based on physical heat transfer modeling of the module and its environment that was accurate to within 1.2 °C for overcast conditions. Luketa-Hanlin and Stein [15] empirically optimized this model for a PV site in Hawaii and found it improved modeling accuracy by as much as 2 °C compared with steady-state models. Lobera and Valkealahti [16] also performed sensitivity analysis and validation of a model similar to the one presented by Underwood and found accuracy within 2 °C for 80% of measured temperature data taken from the TUT Solar

Manuscript received December 9, 2019; revised March 10, 2020; accepted April 15, 2020. Date of publication May 18, 2020; date of current version June 19, 2020. This work was supported in part by the Sandia National Laboratories managed and operated by National Technology & Engineering Solutions of Sandia, LLC, a wholly owned subsidiary of Honeywell International Inc., for the U.S. Department of Energy's National Nuclear Security Administration under contract DE-NA0003525 and in part by the U.S. Department of Energy's Office of Energy Efficiency and Renewable Energy (EERE) under Solar Energy Technologies Office (SETO) Agreement 34366. *(Corresponding author: Matthew Prilliman.)*

Matthew Prilliman and Govindasamy Tamizhmani are with Arizona State University, Mesa, AZ 85212 USA (e-mail: mprillim@asu.edu; manit@asu.edu).

Joshua S. Stein and Daniel Riley are with Sandia National Laboratories, Albuquerque, NM 87122 USA (e-mail: jsstein@sandia.gov; driley@sandia.gov).

Color versions of one or more of the figures in this article are available online at https://ieeexplore.ieee.org.

Digital Object Identifier 10.1109/JPHOTOV.2020.2992351

PV Power Research Test Plant in Tampere, Finland. A model developed by Hayes and Ngan was shown to improve modeling accuracy over 1-min increments by as much as 2 °C [17]. These previous modeling efforts show that there are significant benefits to accounting for transient thermal effects in module temperature prediction, especially in locations with dynamic climatic conditions. The major problem with these physics-based models is that they require parameters that are either not easily available or difficult to measure (e.g., heat transfer coefficients, heat capacities, etc.), they are computationally expensive, and their complexity leads to resistance from industry.

A more useful and easy-to-adapt model would require parameters readily available on a module specification (spec) sheet and be numerically efficient. A weighted moving average is applied on the temperature calculation of a steady-state thermal model to address the need here. Common steady-state models require ambient temperature, irradiance, and wind speed, and the weighted moving average proposed here requires only the mass per unit area (unit mass) from a given module spec sheet and the measured wind speed data at the site. Therefore, only the additional information of a module's area and mass is usually required to apply this model to better represent transient conditions, which are typically available on a spec sheet or easily determined by measurement. Note that the moving-average model is developed for use with planar PV modules where much of the mass is contained in glass on the front and/or rear side of the module.

II. Model Theory

To develop a model that accurately accounts for the thermal mass of the PV module without performing a detailed energy balance of the conductive, convective, and radiative heat transfer mechanisms at every timestep requires a database of module thermal behavior as a basis from which to determine trends in this behavior. This database was generated numerically using 3-D finite-element analysis (FEA) software [18]. Steady-state and transient conditions were simulated on representative modules of varying unit mass to determine how the temperature of a typical PV module would be expected to change under a variety of wind and ambient temperature conditions when presented with a step change in irradiance. The module is assumed to have the properties of a solid sheet of glass as most of a PV module's mass is in the glass for this test case where the metal frame is not considered. The changes in conductivity between glass and other typical module layers such as ethylene vinyl acetate (EVA) encapsulant are neglected for the sake of simplicity. The FEA software allowed for the definition of convective, radiative, and irradiance loads that could be applied on the front and rear surfaces of the module. The geometry of the model was a single PV module in portrait tilted 37° with the lower edge 0.6 m from the ground. The physical assumptions and governing equations used in determining these heat transfer loads are described in the following subsections.

A. Convection

Forced convective cooling (via wind) on a PV module often has the largest impact on module cooling. For the FEA analysis, convection was based on wind hitting the front face of the module at an angle normal to the module surface. As such, the convection on the front surface of the module was assumed to be affected by forced convection, while the rear surface was assumed to experience primarily natural convection. This simplifying assumption was based on a general case in which the racking conditions of the module, and thus, the amount of air flow interacting with the rear surface of the module, was not specified. Full computational fluid dynamic (CFD) analysis was considered to account for and quantify the variations in wind flow turbulence but was ultimately not chosen as it proved to be far more computationally expensive for minimal accuracy gains in comparison to the finite-element method.

The forced convection coefficient used as an input to the FEA software was calculated based on an assumed turbulent wind flow because of the inherent uncertainty in wind direction and wind speed at narrow time scales. The wind was assumed to be measured at a height of 2 m to correspond with common meteorological data collection practices. These assumptions allowed for the use of the following equations for forced convection because of air flow across a flat plate [19]:

$$Nu = 0.0308\mathrm{Re}^{\frac{4}{5}} Pr^{\frac{1}{3}} \tag{1}$$

$$h = \frac{Nu\,(k)}{L} \tag{2}$$

where *Nu* is the Nusselt number, *Re* is the Reynolds number, *Pr* is the Prandtl number, *k* is the thermal conductivity of the air in W/m-K, *L* is the characteristic length of the module in meters, and *h* is the convective heat transfer coefficient because of wind flow across the module surface in W/m^2-K.

For the natural convection on the module backsheet, the convective heat transfer coefficient was calculated based on the approximation of the bottom surface of a vertical hot plate adjusted for a tilt angle of $\theta = 37^\circ$ relative to the ground [19]

$$h = \frac{0.17\left(\left(9.8\cos\left(90-\theta\right)\cdot\left(1/T_f\right)\right)IL^4\right)}{\left(kv^2Pr^2\right)}\cdot\frac{k}{L} \tag{3}$$

where T_f is the film temperature in Kelvin, I is the incident irradiance on the front side of the plate, v is the kinematic viscosity of air in m^2/s, and k is the thermal conductivity of the ambient air in W/(m-K). T_f is found from the average between the surface temperature and the ambient temperature. For this case, the initial surface temperature was calculated from the Sandia module temperature model; a steady-state model using the incident irradiance, wind speed, and ambient temperature as inputs along with empirically determined coefficients in an exponential formula that can be seen in (4) [2]

$$T_m = I\cdot e^{a+WS*b} + T_a \tag{4}$$

where T_m is the module temperature prediction in °C, I is the incident irradiance in W/m^2, WS is the wind speed in m/s, T_a is the ambient temperature in °C, a and b are empirical parameters that depend on the module materials and mounting configuration (e.g., open rack versus close roof mount). A table of representative values for a and b is included in [2].

B. Radiation

In addition to the forced and natural convection loads on the surfaces of the module, the long-wave radiation balance between the module and its environment must be considered. The radiative energy balance between the module surfaces, the sky, and the ground was based on a view factor approach. View factors quantify the amount of thermal radiation passing between two surfaces, with the atmosphere being assumed to be a blackbody surface and the ground having the thermophysical properties of concrete for the sake of this analysis. As the view factors from a given surface to other surfaces, including the viewing surface itself, must add to unity, the view factors of the module's front and back surfaces can be calculated based on an assumed reciprocity between surfaces. This is shown by the following [16], [17]:

$$F_{ij} = \frac{1}{A_j} \iint_{A_1\ A_2} \frac{\cos(\theta_i)\cos(\theta_j)}{\pi R_{ij}^2} dA_i dA_j \tag{5}$$

$$A_i F_{ij} = A_j F_{ji} \tag{6}$$

where F_{ij} is the view factor of surface *i* onto surface *j*, *A* is the area of the respective surface, θ_i is the angle between the surface normal and the line R_{ij} between the two surfaces. Equation (6) shows that reciprocity can be assumed between two surfaces [16], [17].

The ground temperature was calculated by the FEA software based on the material properties of concrete under the varying thermal loads. The sky temperature was calculated based on the following equation from [20]:

$$T_s = T_a * \left(0.711 + 0.0056T_{dp} + 0.000073T_{dp}^2 + 0.013\cos(15t)\right)^{\frac{1}{4}} \tag{7}$$

where T_s is the sky temperature in °C, T_{dp} is the dew point temperature in °C, and t is the hour of the day. t was considered to be at noon for this analysis, while T_{dp} was calculated based on average humidity values for Albuquerque for different seasonal ambient temperature conditions.

As the view factors of the module to both the sky and ground will change with any change in tilt angle, the full range of long-wave radiation effects was not considered in this study. Differences because of tilt angles other than 37° are assumed negligible. This assumption was verified by calculations based on tilt angles ±30° from the initial 37° assumption that resulted in temperatures within 1 °C of the values for the chosen angle.

C. Irradiance

The irradiance incident on the front surface of the glass sheet representing the module was assigned as a time series definition of a heat flux normal to the plane of the glass. For an expected incident irradiance of 1000 W/m^2, the irradiance applied in the FEA was set at 817 W/m^2 to account for heat dissipation because of a solar cell electrical conversion efficiency of 18.3%. For simplification purposes, the irradiance simulation was assumed to be uniform across the entire module (no shading or partial soiling). This FEA process is flexible in that it can be replicated with different heat transfer assumptions or module framing and inclination considerations for specific cases.

TABLE I
STEADY-STATE FEA SIMULATED MODULE BACK-SURFACE TEMPERATURE RESIDUAL COMPARISON TO STEADY-STATE MODEL

-6.7°C Ambient				
Wind speed (m/s)	1	3	5	10
Steady-state model (°C)	19.7	16.0	12.8	6.7
FEA Temperature (°C)	23.9	18.3	14.9	8.2
FEA - Steady (°C)	4.2	2.3	2.1	1.5
15.6°C Ambient				
Wind speed (m/s)	1	3	5	10
Steady-state model (°C)	42.0	38.3	35.1	29.0
FEA Temperature (°C)	40.7	38.2	34.1	28.7
FEA - Steady (°C)	-1.3	-0.2	-1.1	-0.3
32.2°C Ambient				
Wind speed (m/s)	1	3	5	10
Steady-state model (°C)	58.6	54.9	51.7	45.6
FEA Temperature (°C)	57.9	54.3	50.6	45.5
FEA - Steady (°C)	-0.7	-0.6	-1.1	-0.1

III. FINITE-ELEMENT ANALYSIS APPROACH

The FEA simulations were run for different combinations of wind speeds and ambient temperatures and allowed to reach equilibrium. These simulations were validated by comparison to the steady-state Sandia module temperature model, which has been proven to be accurate to measured module temperatures to within 5 °C in previous work [2]. The steady-state simulations were performed at constant wind speeds ranging from 1–10 m/s, ambient temperatures from −7 to 32 °C, and a constant irradiance of 1000 W/m^2 before adjusting for module efficiency to simulate the irradiance under standard module rating conditions [21]. The residuals of the simulated back-surface temperature and the values calculated from the Sandia steady-state model as seen in Table I show convergence within ± 5 °C, which is within the inherent uncertainty of the steady-state model [2]. These results are noteworthy in that they show the ability of the FEA simulation to provide results similar to accepted steady-state thermal models under steady-state conditions.

Upon satisfactory convergence of the FEA simulated temperatures to the steady-state model, FEA simulations with varying irradiance over time were performed to obtain a database of module thermal behavior for several constant wind speed and unit mass conditions. These numerical tests were performed by introducing irradiance step changes of varying sizes across the same range of ambient conditions previously discussed, as well as, across several unit masses. This was done to determine the amount of time needed for the module to reach thermal equilibrium after an irradiance step change from the initial value of 1000 W/m^2. A sample of these transient simulations is shown in Fig. 1.

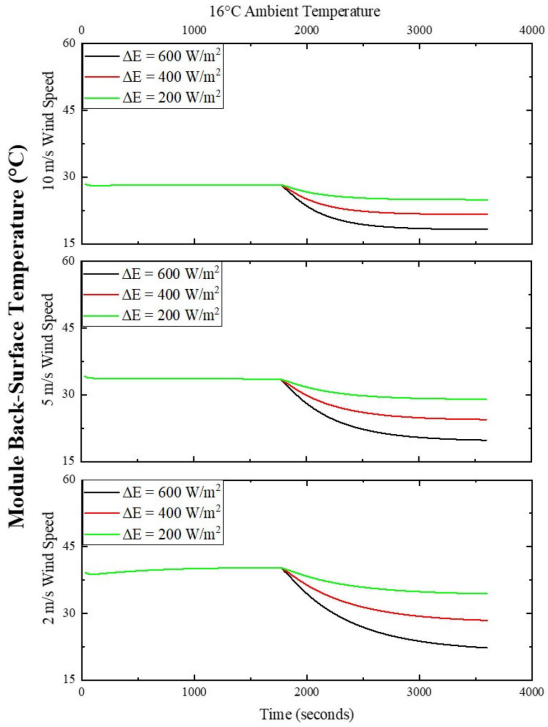

Fig. 1. FEA transient simulations for irradiance step changes.

Analysis of these transient simulations reveals that the rate of change of module temperature for an irradiance step change is exponential with the passage of time. The different ambient conditions serve as a temperature offset to the initial temperature where the step change is introduced but does not affect the exponential behavior of the temperature. The size of the irradiance step change changed the magnitude of the overall decrease in module temperature but had negligible effects on the rate of temperature decay or the time needed to reach 90% equilibrium temperature. As a result of this observed behavior, the exponential temperature curves seen in Fig. 1 are proven to vary primarily with the wind speed rather than the irradiance and ambient temperature. Higher wind speeds flatten the exponential thermal decay, decreasing the amount of time needed for the module temperature to stabilize.

Transient simulations like those shown in Fig. 1 were performed on glass sheets with varying unit mass. The unit mass was varied by increasing the thickness of the glass plate for the same cross-sectional area. Comparison of these curves shows that the time needed for the module temperature to increase or decrease to stabilization increases with increased unit mass because of the higher thermal mass of the module. These results show that the thermal behavior of the module in transient irradiance conditions is dependent on the unit mass and wind speed.

IV. Modeling Methodology

The purpose of the FEA simulations was to create a number of simulated trials of expected PV module temperature changes under simulated irradiance changes with constant wind speed, ambient temperature, and module unit mass. The simulated trials were then analyzed to find trends in module temperature stabilization times and develop a simplified transient thermal model using weighted moving averages. Analysis of the simulated trials indicates that the wind speed and unit mass are the primary parameters in determining the exponential rate of change in module temperature because of irradiance changes that may be expected in field conditions.

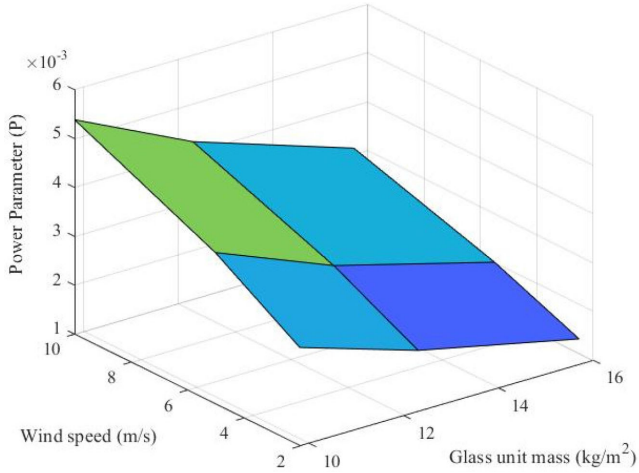

Fig. 2. Surface plot of P values as function of wind speed and unit mass.

Determining the optimum weighting function for the model required fitting the FEA simulated temperatures with an exponential weighting function applied to Sandia steady-state predicted temperatures. This was done by first determining an averaging window size, N, in seconds that defines the number of timesteps backward from the current timestep to include in the moving average. The values in the window are averaged using an exponential weighting function e^{-tP}, where t is the time in seconds back from the timestamp in question and P is the weighting parameter that weights each element in the window. An N value of 1200 s (20 min) was chosen based on the temperature stabilization time in the FEA simulations after introducing a large step change in irradiance. Since the influence of temperature predictions decreases the further back in time from the current timestep, the window can be sized larger than is deemed necessary without significant negative effects on the modeling accuracy.

Once N was set, the exponential weighting function was optimized for the weight parameter P needed to minimize the root mean square error (RMSE) between the moving-average model output and the corresponding transient FEA simulation. This procedure was performed across the range of FEA simulations, and the P parameter found for each simulated wind speed and unit mass condition was plotted as a 3-D surface shown in Fig. 2.

Analysis of the data presented in Fig. 2 reveals that over the typical ranges of wind speed and unit mass, these two parameters have approximately equal effect on the variation of P. Furthermore, the value of P as a function of wind speed and unit mass is roughly planar. As a result of this near equal dependency and planar result, a bilinear interpolation was used to develop a function from which P could be calculated from an

TABLE II
BILINEAR INTERPOLATION COEFFICIENTS FOR MOVING-AVERAGE MODEL

Coefficient	Value
a0	0.0046
a1	0.00046
a2	-0.00023
a3	-1.6E-05

arbitrary wind speed and unit mass. The bilinear interpolation coefficients a_0, a_1, a_2, and a_3 are formed from the following system of equations:

$$\begin{bmatrix} 1 & WS_1 & mu_1 & (WS_1 mu_1) \\ 1 & WS_1 & mu_2 & (WS_1 mu_2) \\ 1 & WS_2 & mu_1 & (WS_2 mu_1) \\ 1 & WS_2 & mu_2 & (WS_2 mu_2) \end{bmatrix} \begin{bmatrix} a_0 \\ a_1 \\ a_2 \\ a_3 \end{bmatrix} = \begin{bmatrix} P_{11} \\ P_{12} \\ P_{21} \\ P_{22} \end{bmatrix}. \quad (8)$$

WS_1 and WS_2 are the lowest and highest wind speeds simulated during the FEA simulations, respectively, with the same syntax that applies to the unit mass *mu* values as well. The P_{ij} values represent the *P* value calculated to fit the model to the FEA analysis done at wind speed *i* and unit mass *j*. The resulting coefficients a_0–a_3 can be used to calculate the weight parameter *P* at any wind speed and unit mass through the following:

$$P = a_0 + a_1 * WS + a_2 * m_u + a_3 * WS * m_u. \quad (9)$$

For the analysis being presented here, these coefficients were found as the values shown in Table II. Recalculating the *P* values via (9) and comparing with measured *P* values shown in Fig. 2 showed *P* prediction accuracy to within 1*e*-5.

With *N* being constant and *P* having been calculated, the full moving-average model can be applied with given module unit mass, measured wind speed, steady-state module temperature predictions, and timestamps. The wind speed data given to the model must be taken from a height similar to the height of the PV modules to match the FEA assumption of wind speed as measured at the PV array. Wind speed measured from any height can be corrected to another height through the log law, which relates the wind speed at different heights through use of a roughness length factor defined by the surrounding environment. This log law relation is shown in (10) [22]

$$v(z) = v(z_r) \frac{\ln\left(\frac{z}{z_0}\right)}{\ln\left(\frac{z_r}{z_0}\right)} \quad (10)$$

where z_r is the measurement (reference) height, *z* is the nominal height of the PV, *v*(*x*) is the wind speed at height of *x*, and z_0 is the surface roughness length. In our analyses, $z_r = 10$ m, z = 2 m, and z_0 was assumed to be 0.25 m based on the table provided in [22].

The simplified inputs to this model, along with optimized code, allow for transient thermal modeling of an annual 1-min dataset in seconds. This optimization was done with the intent of easy integration of the moving-average model into PV performance modeling software packages on top of the existing steady-state temperature models as an optional element of the analysis. The final form of the weighted-moving-average temperature model is shown in (11)

$$T_{MA,i} = \frac{\sum_{i=2}^{t_i \le 1200} \left(T_{SS,i} * e^{-P * t_i}\right)}{\sum_{i=2}^{t_i \le 1200} \left(e^{-P * t_i}\right)} \quad (11)$$

where *i* is the index of a number of prior timesteps, t_i is the number of seconds in the past for each timestep, $T_{SS,i}$ is the steady-state temperature prediction at t_i seconds in the past (°C), and $T_{MA,i}$ is the moving-average model temperature prediction for the current timestep (°C). The model does not use the steady-state model prediction at the current timestep as each sample in the moving average represents the conditions going forward rather than describing conditions from prior times. Under this configuration, using the steady-state temperature at the index being considered would include temperature conditions for periods that have not yet occurred, which would be impossible.

Implementation of the model first requires a calculation of the steady-state temperature predictions being used in the analysis. Then, the model calculates an exponentially weighted moving average of the steady-state temperatures at each timestep where the weighting function is *P*, which is calculated using (9) based on the wind speed measurements for the array site, the unit mass of any module, and the coefficients in Table II. The FEA simulations were performed over a range of unit mass values so that the coefficients in Table II can be used for analysis of a wide variety of PV modules.

At each timestep, the moving-average model calculates the weights for all times within the 1200 s prior to the current time and applies those weights to the steady-state module temperature predictions. Each of these exponentially weighted values are then averaged by the total weight to give the moving-average temperature prediction for the given timestep. This process is repeated for each timestep in the entire dataset. Thus, when the time-series data are presented at timesteps of greater than 10 min and during times with steady irradiance, the moving-average model performs, as well as, the underlying steady-state model. However, when performance data have high temporal resolution and irradiance is varying, the moving-average model smooths out predicted temperature changes with a backward-looking moving average with variable weights.

V. EXAMPLE MODEL IMPLEMENTATION

An example of this model in practice is shown in Table III to serve as a guide and reference implementation for the reader. In this example, data is presented on a 2-min interval for a rectangular module with mass of 18.2 kg and sides of length 1.650 and 0.992 m. The rows of the table indicate the index of each data point relative to index 1, which is the time index for which the module temperature is being calculated. The data between $t = 480$ s and $t = 840$ s is intentionally excluded in this example to show that the model still works for nonuniformly sampled data.

To use the moving-average model in (11), first determine the unit mass of the module being analyzed by dividing the total mass of the module by its one-sided surface area. The surface area used in this calculation is based on only the front surface of

TABLE III
MOVING-AVERAGE MODEL EXAMPLE CALCULATION

Time index, i	SECONDS BEFORE t=0, t_i	Steady State Temp. $T_{SS,i}$ (°C)	2-meter Wind Speed (m/s)	P_i (calculated)	$T_{MA,\,i}$ (calculated) (°C)
1	**0**	**32.5**	**5.0**	**0.0032**	**22.5**
2	120	22.5	-	-	-
3	240	26.2	-	-	-
4	480	28.7	-	-	-
5	840	19.0	-	-	-
6	960	18.2	-	-	-
7	1080	18.3	-	-	-
8	1200	19.0	-	-	-

the module. Here, the unit mass is 11.1 kg/m^2. The unit mass is used along with wind speed adjusted from 10-m measurement height to 2-m PV height with (10) to generate the weighting coefficient P based on the coefficients in Table II via (9).

The numerator in (11) is calculated using the modeled steady-state module temperatures at each index, the P value as determined from the first index, and the time t in seconds from the first index. The denominator in (11) is calculated similarly except the steady-state temperatures are not included. This example results in the moving-average temperature prediction at index $i = 1$. Calculations for the other indices in the dataset would be performed in the same manner. Equation (12) demonstrates how the values in the table are substituted into (11)

$$T_{MA} = \frac{\left[22.5e^{-P*120}\right] + \left[26.2e^{-P*240}\right] + \left[28.7e^{-P*480}\right] + \cdots \left[19.0e^{-P*1200}\right]}{\left[e^{-P*120}\right] + \left[e^{-P*240}\right] + \left[e^{-P*480}\right] + \ldots \left[e^{-P*1200}\right]}. \tag{12}$$

VI. MODEL VALIDATION

Implementing the temperature prediction model described in the previous section provides an added layer of depth to existing thermal models to more effectively predict module or system thermal behavior at fine time scales. The fixed 20-min window over which the weighted moving-average is applied means that the model can greatly improve accuracy over pure steady-state models at data intervals less than 10 min. This is illustrated by empirical cumulative distribution function (CDF) analysis shown in Fig. 3, where a 1-min resolution module daytime temperature dataset from Albuquerque, NM, USA, was subsampled to form datasets with sampling intervals ranging from 1–10 min. The model was then applied to each dataset and compared based on model residuals to measured module temperature data. Fig. 3 shows CDFs of module residuals for each sampling interval.

Inspection of this data reveals that there are substantial benefits when the model is applied over 1-min intervals, and that these benefits gradually decline with increasing time intervals. The 10-min interval is shown to have the same model accuracy as the steady-state model because this interval allows for a moving average of only two prior steady-state predictions at each timestep.

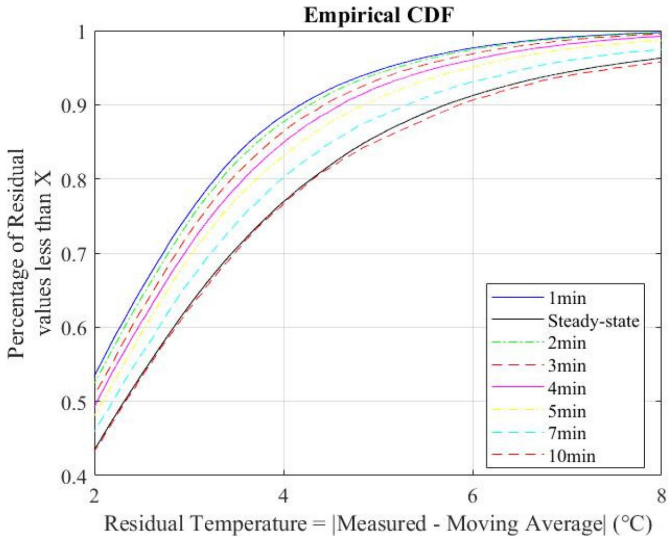

Fig. 3. Empirical CDF of moving-average model residuals.

TABLE IV
FIT STATISTICS FOR MOVING-AVERAGE MODEL AS COMPARED WITH THE SANDIA STEADY-STATE MODEL FOR ANNUAL DATASETS ACROSS 4 LOCATIONS

Albuquerque		
	Optimized SS	Moving-Average
RMSE (°C)	3.79	2.69
MAE (°C)	2.86	2.14
MBE (°C)	-0.442	-0.341
R-Squared	0.936	0.967
Orlando		
	Optimized SS	Moving-Average
RMSE (°C)	4.41	2.03
MAE (°C)	3.02	1.57
MBE (°C)	0.326	0.318
R-Squared	0.880	.975
Vermont		
	Optimized SS	Moving-Average
RMSE (°C)	3.92	2.90
MAE (°C)	2.86	2.20
MBE (°C)	-0.86	-0.83
R-Squared	0.9596	0.977
Las Vegas		
	Optimized SS	Moving-Average
RMSE (°C)	2.86	2.22
MAE (°C)	2.20	1.80
MBE (°C)	-0.380	-0.296
R-Squared	0.968	0.981

With the moving-average filter being shown to considerably improve the modeling accuracy of existing steady-state models, analysis was done to validate the model when applied across various module designs and surrounding climate conditions. Table IV shows the improvement in numerous statistical measures

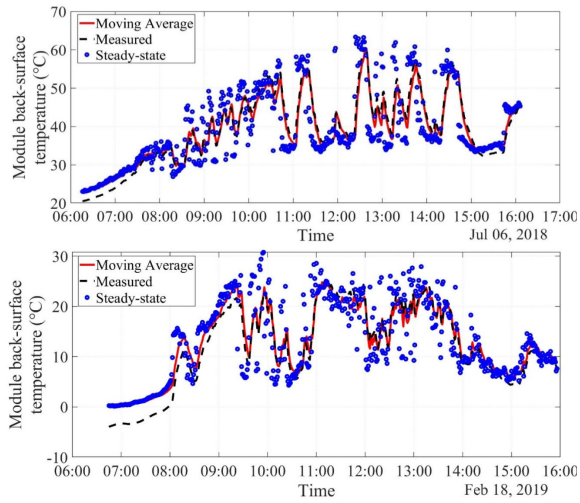

Fig. 4. Summer (top) and winter (bottom) moving-average model versus steady-state predictions and measured module temperatures for Albuquerque, NM, USA.

of the moving-average model's fit to 1-min measured module temperature data over a full year for sites in Albuquerque, NM, Orlando, FL, Las Vegas, NV, and Williston, VT. The model performance was analyzed in terms of the RMSE, the mean absolute error (MAE), the mean bias error (MBE), and the R^2 coefficient of fit between the modeled time-series temperature data and the measured data. The steady-state model used for this analysis was the Sandia steady-state model with model coefficients that were optimized for each site by minimizing the RMSE between steady-state predicted temperatures and measured module temperatures. The steady-state model optimization required finding coefficients for each climate condition that minimized the RMSE for time stamps determined to be under clear sky daytime conditions where there was negligible intermittency in the incident irradiance. The resulting optimized steady-state model was also used in the calculation of the moving-average model temperature predictions. The effect of using nonoptimized parameters (e.g., parameters suggested in [2]) would simply result in a modest temperature offset of a few degrees but would have very little effect on the resulting temperature variability with time.

Inspection of these metrics before and after the application of the moving-average filter shows that the modeling performance improvement from pure steady state to moving-average model is greatest for regions such as Orlando and Florida that experience many partly cloudy days that cause greater intermittency in solar resource. The negative MBE values for each system except Orlando show that there is a slight overprediction bias that can be attributed to inaccuracies in the steady-state model. Visual inspection across random days in these datasets shown in Fig. 4 reveals that the model closely follows the shape of the measured temperature data at an offset driven by inherent inaccuracies in the steady-state model.

Histogram analysis of the model residuals for similar modules installed at four different test sites is shown in Fig. 5. These histograms show the majority of the model temperature predictions to be within 2 °C of the measured temperature data for different

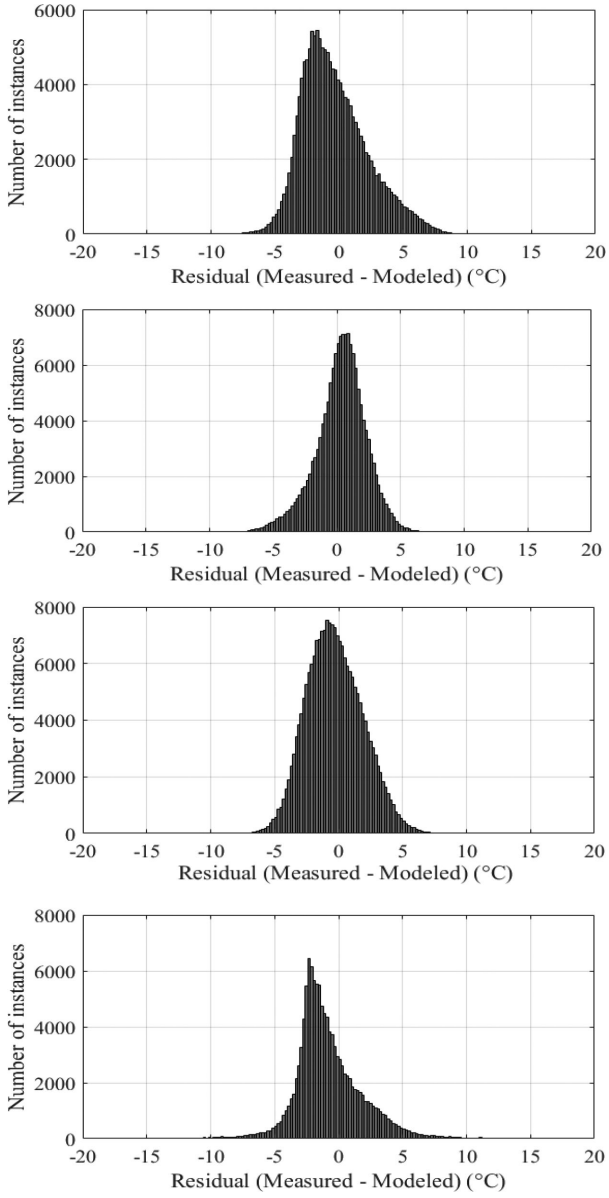

Fig. 5. Histogram of moving-average model residuals for, from top: Albuquerque, Orlando, Las Vegas, and Williston.

climates. Considering the inherent uncertainty of the Sandia steady-state model [2], these results are within a satisfactory range to be trusted in energy performance calculations. This histogram analysis further exemplifies the usefulness of this moving-average model, as it requires only simple analytical interpolation to greatly improve the accuracy of existing steady-state models without complex empirical analysis.

Ultimately, the PV industry will judge the effectiveness and usefulness of the model primarily on how it improves the accuracy of energy prediction performance models such as those in software packages that can simulate PV performance at timesteps finer than 10 min. Adding the moving-average filter on top of the steady-state models currently employed in these software packages allows for more accurate module temperature predictions at short time scales, and thus, results in more accurate estimates of the energy production of PV plants.

Using the improvements in MAE for the moving-average model as shown in Table IV and an assumed temperature coefficient for power production of $-0.4\%/°C$ led to estimated energy accuracy improvements ranging from 0.17% for the clear skies of Las Vegas to 0.58% for the more intermittent skies of Orlando. Such improvement in accuracy is similar to that provided by the physical transient thermal model presented by Hayes and Ngan [17]. Performance gains of this scale can make a significant financial impact on the design of utility-scale PV systems.

VII. Conclusion

This article presents a new PV module back-surface temperature model that exponentially weights steady-state temperature predictions from previous timesteps. FEA simulations were run to produce sample trial predictions of module temperature change because of irradiance changes under constant wind speed. Based on the cooling rate of PV modules in the FEA simulations, a range of exponential weighting values was determined as a function of wind speed and PV module unit mass. This range of exponential weighting values is determined for arbitrary unit mass and wind speed by bilinear interpolation for use within the weighted moving-average temperature model. The model can be used as an improvement upon any steady-state temperature model and does not add significant computation time to PV performance models.

Validation of this model's accuracy shows that it is able to improve modeling accuracy and reduce residual variability across numerous climate conditions, particularly those characterized by intermittent solar resource. These improvements in temperature modeling performance were also shown to have up to a 0.58% improvement on the accuracy of overall PV system annual energy models, thus proving valuable for future system development and analysis. The moving-average model can add significant value to the current state of PV module temperature prediction for those who desire to have more accuracy at high temporal resolution without the complex calculations and hard-to-find input data of a full physical heat transfer model.

The moving-average model implementation and validation presented here serve to account for the thermal mass of the module while still utilizing existing steady-state models. Dependence on these models causes their inherent uncertainties to be passed on to the transient prediction. Improving the accuracy of the moving-average model beyond what has been presented here would require empirical determination of the effects of previously unaccounted for environmental parameters in steady-state modeling such as wind direction and sky temperature. Additionally, improvements in the moving-average weighting would stem from more detailed FEA simulations for specific mounting and module material considerations. These factors, along with any others with significance on PV temperature prediction, will be considered in future modeling efforts. While the model presented in its current state does offer a realistic prediction of the module surface temperature, these further efforts would magnify the accuracy gains of this model to an, even greater degree. The model as presented here will be available in PVLIB and any further modeling efforts will be made available once validated [23].

References

[1] K. Mertens, *Photovoltaics: Fundamentals, Technology, and Practice*. Hoboken, NJ, USA: Wiley, 2014.

[2] D. L. King, J. A. Kratochvil, and W. E. Boyson, "Photovoltaic array performance model," Sandia Nat. Lab., Albuquerque, NM, USA, Rep. SAND2004-3535, Aug. 2004.

[3] D. Faiman, "Assessing the outdoor operating temperature of photovoltaic modules," *Prog. Photovolt. Res. Appl.*, vol. 16, pp. 307–315, 2008.

[4] A. Q. Malik and S. J. B. H. Damit, "Outdoor testing of single crystal silicon solar cells," *Renew. Energy*, vol. 28, no. 9, pp. 1433–1445, 2003.

[5] J. M. Servant, "Calculation of the cell temperature for photovoltaic modules from climatic data," in *Proc. 9th Biennial Congr. Int. Solar Energy Soc.*, vol. 3, 1986, pp. 1640–1643.

[6] S. C. W. Krauter, "Development of an integrated solar home system," *Sol. Energy Materials Sol. Cells*, vol. 82, no. 1/2, pp. 119–130, 2004.

[7] T. Nordmann and L. Clavadetscher, "Understanding temperature effects on PV system performance," presented at the *3rd World Conf. Photovolt. Energy Convers.*, Osaka, Japan, vol. C, May 11–18, 2003, pp. 2243–2246.

[8] C. Hansen, J. S. Stein, and D. Riley, "Effect of time scale on analysis of PV system performance," Sandia Nat. Lab., Albuquerque, NM, USA, Rep. SAND2012-1099, Feb. 2012.

[9] S. Ransome and P. Funtan, "Why hourly averaged measurement data is insufficient to model PV system performance accurately," presented at the *20th Eur. Photovolt. Solar Energy Conf.*, Barcelona, Spain, Jun. 6–10, 2005.

[10] J. Good and J. X. Johnson, "Impact of inverter loading ratio on solar photovoltaic system performance," *Appl. Energy*, vol. 177, pp. 475–486, 2016.

[11] M. J. Reno, M. Lave, J. E. Quiroz, R. J. Broderick, and S. N. Laboratories, "PV ramp rate smoothing using energy storage to mitigate increased voltage regulator tapping," Sandia Nat. Lab., Albuquerque, NM, USA, Rep. SAND2016-5509, 2016.

[12] S. Armstrong and W. G. Hurley, "A thermal model for photovoltaic panels under varying atmospheric conditions," *Appl. Therm. Eng.*, vol. 30, no. 11–12, pp. 1488–1495, 2010.

[13] K. Sayed, M. Abdel-Salam, M. Ahmed, and A. A. Ahmed, "Electro-Thermal Modeling of Solar Photovoltaic Arrays," presented at the *ASME 2011 Int Mech. Eng. Congr. Expo.*, Denver, Colorado, USA, November 11–17, 2011.

[14] A. D. Jones and C. P. Underwood, "A thermal model for photovoltaic systems," *Sol. Energy* vol. 70, no. 4, pp. 349–359, 2001.

[15] A. Luketa-hanlin and J. S. Stein, "Improvement and validation of a transient model to predict photovoltaic module temperature," Sandia Nat. Lab., Albuquerque, NM, USA, Rep. SAND2012-5509, 2012.

[16] D. T. Lobera and S. Valkealahti, "Dynamic thermal model of solar PV systems under varying climatic conditions," *Sol. Energy*, vol. 93, pp. 183–194, 2013.

[17] W. Hayes and L. Ngan, "A time-dependent model for CdTe PV module temperature in utility-scale systems," *IEEE J. Photovolt.*, vol. 5, no. 1, pp. 238–242, 2015.

[18] Dassault Systemes Solidworks Corporation, Vélizy-Villacoublay, France, Solidworks 2017. [Online]. Available: www.solidworks.com

[19] J. P. Holman, *Heat Transfer*, 10th ed., London, U.K.: McGraw-Hill, 2010.

[20] J. A. Duffie and W. A. Beckman, *Solar Engineering of Thermal Processes*. 4th ed., Hoboken, NJ, USA: Wiley, 2013.

[21] *Terrestrial Photovoltaic (PV) Modules - Design Qualification and Type Approval—Part 2: Test Procedures*, IEEE Standard 61215, 2016.

[22] J. F. Manwell, *Wind Energy Explained: Theory, Design, and Application*, 2nd ed., Hoboken, NJ, USA: Wiley, 2003.

[23] W. Holmgren, C. Hansen, and M. Mikofski, "Pvlib python: A python package for modeling solar energy systems," *J. Open Source Softw.*, vol. 3, no. 29, 2018, Art. no. 884.